Article

Pt catalyzed aqueous-phase hydrogenation of D-glucose to D-sorbitol

Xingguang Zhang, Lee J Durndell, Mark A. Isaacs, Christopher M. A. Parlett, Adam F. Lee, and Karen Wilson

ACS Catal., **Just Accepted Manuscript** • DOI: 10.1021/acscatal.6b02369 • Publication Date (Web): 26 Sep 2016

Pt catalyzed aqueous-phase hydrogenation of D-glucose to D-sorbitol

Xingguang Zhang,[†] Lee J. Durndell,[†] Mark A. Isaacs,[†] Christopher M.A. Parlett, [†] Adam F. Lee,[†] and Karen Wilson[†]**

[†]European Bioenergy Research Institute, Aston University, Birmingham B4 7ET, UK.

ABSTRACT. Aqueous phase hydrogenation of D-glucose to D-sorbitol was systematically investigated over silica supported Pt nanoparticles to elucidate structure-reactivity relations and mechanistic insight. D-glucose hydrogenation over large Pt particles competes with its isomerization to D-fructose over low coordination (electron deficient) Pt sites; D-sorbitol production by the former process was structure insensitive for nanoparticles spanning 3-17 nm, whereas isomerization was favored by smaller particles, with both pathways independent of the choice of fumed silica or mesoporous SBA-15 support. While D-fructose was readily hydrogenated to D-mannitol under the same reaction conditions, the latter underwent minimal isomerization to D-sorbitol which is thus a direct product of D-glucose ring-opening and subsequent hydrogenation of the aldose conformer. D-sorbitol production was favored by low D-glucose concentrations <10 wt%, high H_2 pressures >40 bar and low reaction temperatures <140 °C, which suppressed undesired polymerization side reactions.

KEYWORDS: Glucose; Hydrogenation; Platinum; Sorbitol; SBA-15.

1. INTRODUCTION

Carbohydrates derived from lignocellulosic biomass waste, such as agricultural or forestry residues and the organic fraction of municipal solid waste, are an attractive source of biogenic carbon from which to derive sustainable biofuels and platform chemicals.[1-5] In 2004, D-sorbitol was identified as one of the 12 most important value added chemicals obtainable from biomass by the US Department of Energy, as a potential source of alkanes for liquid biofuels, or "outstanding building block for commodity chemicals", notably through its dehydration to isosorbide.[6,7] Esters and derivatives of D-sorbitol also represent important additives and

intermediates in the cosmetics and pharmaceuticals sectors, with the molecule a key sugar substitute in the food and beverage industry, with an annual global production ~800,000 tons.[6,7]

D-Sorbitol is commonly obtained through the transition metal catalyzed hydrogenation of D-glucose,[8] notably over Ni[9,10 11,12], Ru,[13-16,17] Pt[18] and Rh[10] supported on oxides, carbons, polymers, hydrotalcites and zeolites. Commercial processes typically employ either Raney Ni or carbon supported Ru catalysts, however the former offers relatively poor selectivity and are prone to progressive on-stream deactivation and product contamination,[12] while the latter is expensive and susceptible to poisoning by strongly bound organic impurities or sulfur compounds.[19] Obviously the existence of a commercial catalytic process must not preclude the pursuit of further process improvements and advancement of fundamental scientific knowledge, and hence studies have explored the role of basic supports, or poorly reduced active phases, in promoting the Canizzaro side reaction and concomitant gluconic acid formation,[20] a possible contributor to the deactivation of Ni and Ru catalysts.[21] The influence of dopants to improve activity and selectivity,[11] such as Ru-B,[22] Ni-P[23] and Co-B,[24] has also been exploited, however the resulting catalysts possess low surface areas and poor thermal stability, underperforming Raney Ni in industrial application. Pt nanocatalysts are generally more reducible and offer greater stability under hydrothermal reaction conditions than Ni or Ru, and exhibit excellent performance in hydrogenation and hydroisomerization reactions.[25,26,27] Gallezot et al demonstrated continuous glucose hydrogenation to sorbitol in high yields over Ru/C,[17] but employed high H_2 pressures (80 bar) and a 40 wt% glucose solution more concentrated than likely to be available from biorefineries through e.g. steam explosion wherein the resulting hydrolysate and condensate comprise ~1-10 wt% glucose,[28] and 8-15 g catalyst charges in the fixed bed. Sorbitol yields from Ru supported on alumina and titania are far lower in batch, typically 20-60 % even at 120 bar hydrogen.[12] In contrast, Perrard and co-workers[18] reported 10 wt% Pt/C catalysts operating at 100 °C and 80 bar H_2 pressure with a specific activity of 1800 $mmol \cdot g_{Pt}^{-1} \cdot h^{-1}$ and selectivity >99.5 % to D-sorbitol. Hydrotalcite addition to the reaction medium dramatically enhanced both glucose hydrogenation and concomitant sorbitol production over a 3.5 wt% Pt/Al_2O_3 catalyst, attributed to enhancement of open chain form glucose under alkaline conditions.[29] The only direct comparative studies of glucose hydrogenation over low loading Ru and Pt on activated carbon reported identical activities between the two metals in both batch and flow operation, but superior sorbitol selectivity for platinum in all cases.[30,31]

Unfortunately, none of the preceding studies employed reaction conditions free from mass transport limitations or reported carbon mass balances, prohibiting reliable and quantitative assessment of the influence of either catalyst properties or operating conditions, or comparisons between catalysts.

Despite the potential significance of Pt catalyzed carbohydrate hydrogenation[32-35] for biorefining, the aqueous phase hydrogenation of D-glucose to D-sorbitol therefore remains poorly understood, with no systematic studies into the reaction network or structure sensitivity, or performance benchmarking of intrinsic reaction rates. Here we report the first fundamental investigation into structure-activity relationships for aqueous phase glucose hydrogenation by any family of well-defined and systematically-related catalysts, identifying strong particle size and support effects for silica supported Pt catalysts. Such insight will prove valuable for the development of more robust, active and selective catalysts for the overall hydrolytic hydrogenation of cellulose to sugar alcohols,[36] an important route to improve the efficiency of biomass conversion to platform chemicals and fuels.[37,38]

2. EXPERIMENTAL

Catalyst synthesis

Two families of fumed silica and SBA-15 supported Pt catalysts were prepared by wet impregnation.[39] Typically, 2.5 g of the support (SBA-15 or fumed silica) was contacted with 25 mL aqueous ammonium tetrachloroplatinate(II) solution with the metal precursor concentration adjusted to achieve nominal Pt loadings spanning 0.05-2 wt%. Slurries were stirred for 18 h overnight at room temperature, and subsequently evaporated to dryness at 80 °C under agitation. The resulting powders were calcined at 550 °C for 2 h under static air in a muffle furnace (ramp rate 1 °C.min^{-1}), followed by reduction at 400 °C for 2 h (ramp rate 10 °C.min^{-1}) under flowing H_2 (10 mL.min^{-1}). Catalysts were stored under ambient conditions and used for reactions without further treatment.

Catalyst characterization

Nitrogen porosimetry was undertaken on a Quantachrome Nova 4000e porosimeter and analyzed with NovaWin software version 11. Samples were degassed in vacuo at 120 °C for 2 h prior to measurement of nitrogen adsorption/desorption isotherms at -196 °C. BET (Brunauer-

Emmett-Teller) surface areas were calculated over the relative pressure range 0.01-0.2. Pore diameters and volumes were calculated by applying the BJH method to desorption isotherms for relative pressures >0.35. Low and wide angle XRD patterns were recorded on a Bruker D8 Advance diffractometer fitted with a LYNXeye detector and Cu K_α (1.54 Å) calibrated against a corundum standard. Low angle patterns were recorded from 2θ = 0.45-8 ° with a step size of 0.01 °, and wide angle patterns from 2θ = 20-90° with a step size of 0.02 °. The Scherrer equation was used to calculate volume-averaged Pt crystallite diameters from broadening of the associated fcc metal reflections. XPS was performed on a Kratos Axis HSi X-ray photoelectron spectrometer fitted with a charge neutralizer and magnetic focusing lens, employing Al K_α monochromatic radiation (1486.7 eV). Spectral fitting was performed using CasaXPS version 2.3.14. Binding energies were corrected to the C 1s peak at 284.6 eV and surface atomic compositions calculated via correction for the appropriate instrument response factors. Pt 4f XP spectra were fitted using a Doniach Sunjic modified Gaussian-Lorentzian asymmetric lineshape. Pt dispersions were measured via CO pulse chemisorption on a Quantachrome ChemBET 3000 system. Samples were outgassed at 150 °C under flowing He (20 $mL.min^{-1}$) for 1 h, prior to reduction at 150 °C under flowing hydrogen (10 $L.min^{-1}$) for 1 h before room temperature analysis in order to remove any surface oxide formed during storage; this reduction protocol is milder than the 400 °C reduction employed catalyst synthesis, and does not induce particle sintering and hence avoids distortion of the true Pt dispersion in the as-prepared catalyst. A CO:Pt surface stoichiometry of 0.68 was assumed,[40 41] since the formation of a fully saturated monolayer is energetically unfavorable under the measurement conditions employed. Powder XRD and TEM on spent catalysts revealed no evidence of in-situ particle sintering during the liquid phase hydrogenation of D-glucose under our (relatively mild) standard reaction conditions of 40 bar and 140 °C. Scanning transmission electron microscopy (STEM) was conducted on an aberration corrected JEOL 2100-F electronic microscope operating at 200 kV, with mean Pt particle sizes determined from a minimum of 100 particles. Elemental analysis of the bulk Pt content of digested samples was measured by ICP-OES using a VARIAN VISTA MPX instrument (MEDAC Ltd).

D-glucose hydrogenation

D-Glucose hydrogenation was performed in a 50 mL stainless steel Parr autoclave using 40 mL of 2.5 wt% D-glucose aqueous solution, typically at 140 °C and 40 bar H_2 pressure. Reactions were performed for 4 h under 900 rpm stirring (which tests confirmed sufficient to eliminate external mass transport limitations, **Figure S6c**). In a typical protocol, 0.2 g catalyst was added to the reaction mixture and the reactor purged with N_2 three times to remove oxygen, and an aliquot removed. The reaction mixture was subsequently heated to the target temperature under N_2 and immediately sampled again to assess whether significant reaction occurred during the (approximately 20 min) heating process. Finally, the autoclave was filled to a constant H_2 pressure, maintained from an external manifold, and aliquots periodically removed via a dip-tube inserted into the solution, filtered to remove catalyst, and then analyzed without dilution by a 1200 Infinity Series Agilent Technologies HPLC equipped with a refractive index detector and Hi-Plex Ca-Duo column at 80 °C using a pure water mobile phase at 0.6 mL.min^{-1}. Analyses were performed in triplicate, with a peak area reproducibility of ±2 % for D-glucose, D-fructose and D-sorbitol, and ±10 % for D-mannitol due to its extremely low yield. Response factors for D-glucose, D-mannose, D-fructose, D-mannitol and D-sorbitol were determined from respective multi-point calibration curves. D-glucose conversion, product selectivity and yield, and carbon mass balances were calculated according to Equations 1 to 4 below:

$$\text{Conversion / \%} = \frac{(\text{Moles of glucose}_{t=0} - \text{Moles of glucose}_{t=\text{i}})}{\text{Moles of glucose}_{t=0}} \times 100 \quad \text{Eq. 1}$$

$$\text{Selectivity / \%} = \frac{\text{Moles of product}}{(\text{Moles of glucose}_{t=0} - \text{Moles of glucose}_{t=\text{i}})} \times 100 \quad \text{Eq. 2}$$

$$\text{Yield / \%} = \frac{\text{Moles of product}}{\text{Moles of glucose}_{t=0}} \times 100 \quad \text{Eq. 3}$$

$$\text{Mass balance / \%} = \frac{\text{Total moles of carbon in all products}}{\text{Moles of carbon in converted glucose}} \times 100 \quad \text{Eq. 4}$$

Initial reaction rates of D-glucose conversion and D-sorbitol production were determined at low conversion (<25%) from the linear portion of reaction profiles, i.e. in the absence of mass-transport limitations or catalyst deactivation, and used to calculate Turnover Frequencies (TOFs)

for D-glucose conversion and D-sorbitol productivity based upon the number of surface Pt atoms determined by CO chemisorption. Initial rates of D-fructose, D-mannitol and D-sorbitol conversion as reactants were likewise were determined at low conversion (<25%). Selectivities are reported at iso-conversion levels of approximately 5 % unless otherwise specified.

3. RESULTS AND DISCUSSION

Catalyst characterization

The successful genesis of Pt impregnated SBA-15 having an ordered hexagonal close packed mesoporous network was confirmed by low angle XRD and nitrogen porosimetry (**Figure S1**). Three well resolved reflections at 2θ = 0.96, 1.57 and 1.8°, characteristic of the (1 0 0), (1 1 0) and (2 0 0) planes of the *p6mm* symmetric SBA-15 support architecture, were visible in both the parent and Pt functionalized materials. Nitrogen porosimetry showed the expected type IV isotherm with H1 hysteresis loop characteristic of SBA-15 for all Pt loadings, with a common mean BJH pore diameter of 6.7 nm indicating that silica mesoporous channels remained unblocked following Pt impregnation. Pt/fumed silicas prepared from a commercial amorphous support exhibited a type II N_2 adsorption isotherm, consistent with a low surface area non-porous or macroporous material. BET surface areas for both silica families decreased with increasing Pt loading, with the Pt/SBA-15 samples exhibiting the greatest losses (up to 15 %) compared with the parent support. Pore volumes of SBA-15 also declined slightly with increasing Pt loading, which we attribute to partial blockage of micropores within the mesopore walls.[18] It is important to note that these small decreases indicate that the majority of mesopore channels and entrained Pt nanoparticles remain fully accessible to reactants; porosimetry (an averaging methodology not susceptible to the selective bias inherent in spatially-localized electron microscopy) confirms that SBA-15 mesopores were not blocked by Pt. The small decrease in surface areas for the Pt/fumed silica samples was consistent with deposition of Pt nanoparticles predominantly over the external surface area of the amorphous support (**Table S1**).

Wide-angle XRD patterns of SBA-15 and commercial SiO_2 families of Pt catalysts show reflections at 2θ = 39.8°, 46.4° and 67.6° (**Figure S2**) associated with the (111), (200) and (220) facets respectively of fcc Pt metal. The decrease in FWHM of these reflections with Pt loading is indicative of a concomitant increase in Pt cluster size for both supports, quantified by Scherrer analysis (**Figure 1a**). In general, the high area SBA-15 support favors smaller Pt particle sizes

(and correspondingly higher dispersions from CO chemisorption, **Figure S3**) for a given metal loading than the fumed silica, with values in excellent agreement with those measured by STEM (**Tables S1-2** and **Figure S4**): the average Pt particle size varied from 3.8-10.5 nm for Pt/SBA-15 and 3.4-16.6 nm for Pt/fumed silica. Pt 4f XP spectra of the Pt/SBA-15 series (**Figure S5**) revealed a monotonic increase in surface Pt concentration with bulk Pt loading shown in **Figure 1b**. Corresponding Pt surface concentrations for the Pt/fumed silica family mirror those for the SBA-15 support for bulk Pt loadings ≤0.4 wt%, above which they attained a plateau consistent with formation of the large three-dimensional Pt crystallites observed by XRD. Peak fitting of both Pt/SBA-15 and Pt/fumed silica families demonstrated that platinum was predominantly present in metallic form (composition spanning 80-95 % Pt^0) for all loadings.

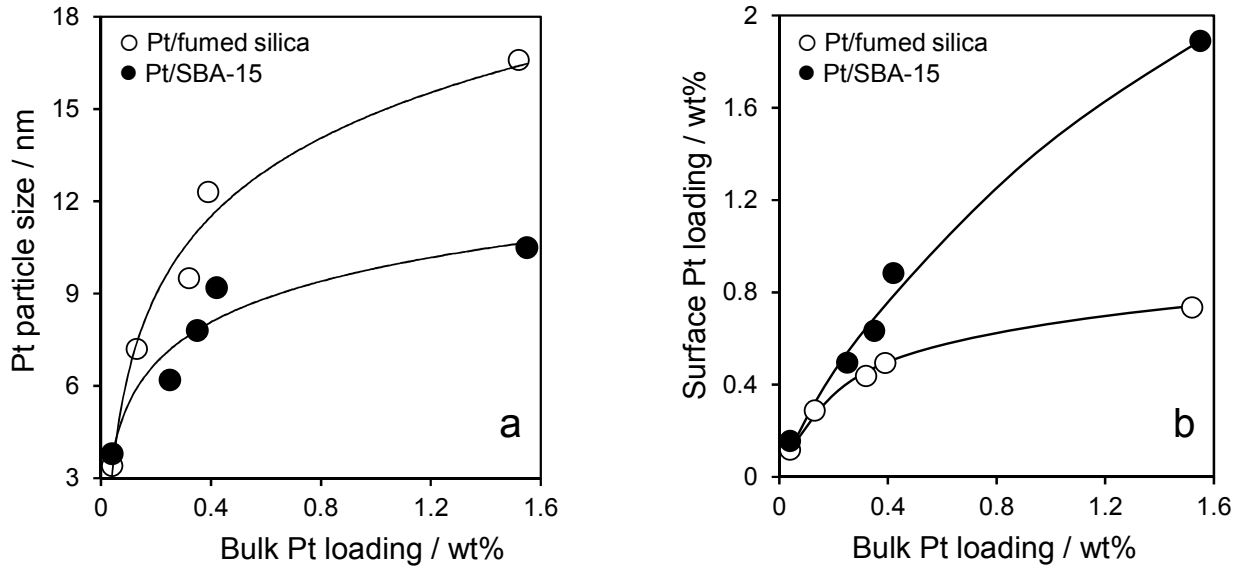

Figure 1. Influence of (a) Pt particle size and (b) surface Pt content from XPS with bulk Pt loading over SiO_2 and SBA-15 supports.

D-Glucose hydrogenation

i) Structure-activity relationships

The influence of Pt particle size on the aqueous phase hydrogenation of D-glucose was initially investigated under 140 °C and 40 bar (conditions favoring good hydrogenation activity and D-sorbitol formation as discussed later, and under which the catalyst charge and agitation rates were chosen to ensure freedom from mass-transport limitations, see **Figure S6a-c**). Activities for D-glucose conversion (**Figure S7a**) were inversely proportional to Pt particle size, i.e. rate $\propto$ diameter^{-y}, with proportionality constants y >1 over both supports, indicating that the rate of D-

glucose conversion is not directly correlated with the geometric surface Pt atom density, i.e. *at least one of the possible reaction pathways for D-glucose is structure sensitive*. The highest specific activities for D-glucose conversion of 1 and 1.5 $mol.g^{-1}_{Pt}.h^{-1}$, observed for the smallest (3.4 nm) Pt particles on SiO_2 and SBA-15 respectively, are in good agreement with that reported at 100 °C but a significantly higher 80 bar H_2 pressure for 4 nm Pt particles on activated carbon cloth,[18] and significantly higher than reported by Gallezot et al of 342 $mmol.g_{Ru}^{-1}.h^{-1}$ over 1.8 wt% Ru on activated carbon extrudates.[17] It should be noted that the literature on metal catalyzed glucose hydrogenation is dominated by an inappropriate focus on sorbitol % yield, which is a very poor measure of catalyst performance since it is entirely dependent on the chosen reaction conditions (particularly catalyst:substrate ratio and timescale of reaction), and hence is not a transferable parameter between studies. D-sorbitol productivity, expressed as either $mmol.g^{-1}_{metal}.time^{-1}$ or Turnover Frequency (TOF) per amount of metal, is a far more meaningful parameter for catalyst comparison.

The primary products from D-glucose were D-fructose and D-sorbitol over all catalysts, with D-fructose productivity semi-quantitatively mirroring the Pt size dependence of D-glucose conversion (**Figure S7b**), suggesting that isomerization of the latter is the dominant process under these initial reaction conditions, and that Pt is structure sensitive for this transformation (possibly catalyzed by Lewis acid $Pt^{\delta+}$ sites present on smaller particles). In contrast, while D-sorbitol productivity was likewise inversely proportional to Pt particle size, the proportionality constants *y* were close to unity over both supports (**Figure 2a**), as would be anticipated if D-sorbitol production depended solely on the geometric Pt surface area, i.e. if *D-glucose hydrogenation to D-sorbitol is structure insensitive*. This hypothesis was confirmed by calculating the TOFs for D-sorbitol production (normalized to the surface Pt metal), which **Figure 2b** reveals as both support and particle size invariant across the particle size range investigated. Our observed TOFs of 45-60 h^{-1} are in good agreement literature values of 54 h^{-1} and 75 h^{-1} reported for Pt/Al_2O_3[29] and Ru/SiO_2[42] respectively.

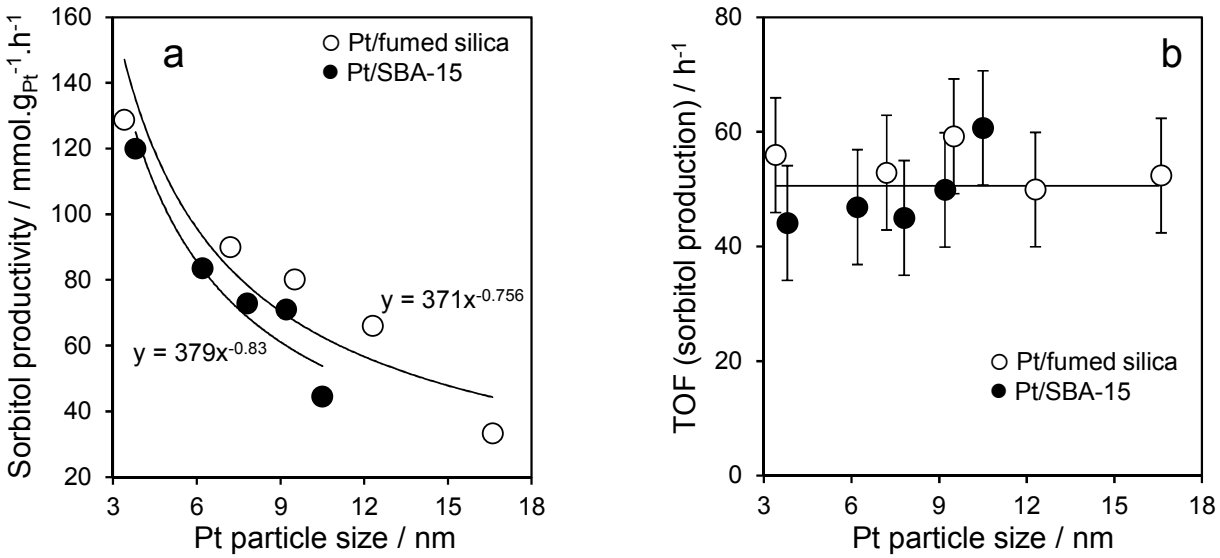

Figure 2. Influence of Pt particle size on (a) sorbitol productivity, and (b) sorbitol TOF during aqueous phase glucose hydrogenation over silica and SBA-15 supports at 140 °C and 40 bar.

The preceding results indicate that D-glucose isomerization to D-fructose is favored over low coordination $Pt^{\delta+}$ sites which XPS fitting reveals are more prevalent on smaller particles (**Figure S8**), whereas sorbitol formation is structure insensitive, hence selectivity towards these products is expected to exhibit a particle size dependence at iso-conversion. **Figure 3** confirms this prediction, with D-sorbitol selectivity rising approximately linearly with Pt particle size (and loading) at the quantitative expense of D-fructose over both supports, consistent with competing reaction pathways. Recycle tests, performed on the 5 wt% Pt/SBA-15 catalyst without any reactivation protocols, demonstrated good stability, with 75 % of sorbitol productivity retained on re-use; the slight activity loss is attributed to carbon deposition, with CHNS revealing ~3 wt% carbon in the spent catalyst, likely arising from strongly-adsorbed oligomers of reactively-formed fructose[43] or associated 5-hydroxymethylfurfural (5-HMF).[44] The issue of catalyst stability during glucose hydrogenation is very rarely addressed in literature reports, and in all but one case (the study by Sapunov et al[16]) quantitative comparison is in any event hindered by: (i) the failure to report mass balances; and (ii) the decision to operate under forcing reaction conditions with a view to achieving complete glucose conversion/high sorbitol yields, the wrong regime in which to assess deactivation (**Table 1**) since reactions are mass transport limited (and susceptible to product inhibition) rather than reaction rate limited.

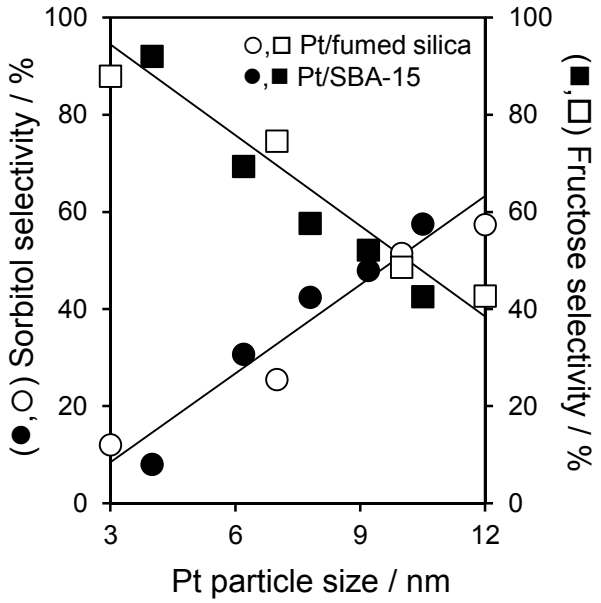

Figure 3. Influence of Pt particle size on sorbitol and fructose selectivity during aqueous phase glucose hydrogenation over silica and SBA-15 supports at 140 °C and 40 bar. Selectivities calculated at 5 % glucose conversion.

Table 1. Comparison and limitations of representative metal catalyzed D-glucose hydrogenation.

Catalyst	1st cycle conversion or yield[a] / %	Recycle	Carbon mass balance	Reaction conditions	Ref.
Ru/mesoporous carbon microfibers	N.R.[b]	Stable over 5 cycles	N.R.	40 wt% glucose, 0.05 g catalyst, 100 °C, 80 bar, 3 h, 1000 rpm, 30 mL	13
Ru/MCM-41	>97	15 % sorbitol yield loss after 1 cycle	N.R.	10 wt% glucose, 0.25 g catalyst, 120 °C, 30 bar, 3 h, 500 rpm, 25 mL	15
Ru/Polystyrene	41	Stable over 10 cycles	N.R.	29 wt% glucose, 0.4 g catalyst, 100 °C, 40 bar, 1.33 h, 50 mL	16
1 wt% Ru/HY	>95	~5 % activity loss after 1 recycle. TEM evidenced aggregation	N.R.	25 wt% glucose, 1 g catalyst, 120 °C, 55 bar, 0.33 h, 1200 rpm, 160 mL	14
Ru/ZSM-5-TF	>95	~5-20 sorbitol yield loss after 1 recycle.	N.R.	25 wt% glucose, 0.5 g catalyst, 120 °C, 40 bar, 2 h, 500 rpm, 50 mL	45
Ru(1%)/NiO(5%)-TiO_2	>93	Not reported	N.R.	20 wt% glucose, 120 °C, 55 bar, 2 h, 1200 rpm	46
5 wt% Pt/charcoal	>94	5 % sorbitol yield loss after 5 recycles	N.R.	25-65 °C, 1 bar., 10 wt% glucose, 12 wt% catalyst	47
Pt-PEI nanoparticles	100	Not reported	'Poor'	0.48 g glucose, 60 g water, 1 g Pt-PEI dispersion, 50 bar H_2, 3 h, 180 C	48
1 wt% Pt/AC	>95	Not reported	N.R.	2.8 wt% glucose, 0.06 g catalyst, 180 °C, 16 bar, 3 h, 1100 rpm, 5 mL	30
10 wt% Pt/AC cloth	~100	Not reported	N.R.	40 wt% glucose, 100 °C, 80 bar, catalyst mass unreported	18
Pt/γ-Al_2O_3 + 0.075 g Hydrotalcite	100	20 % activity loss after 1 cycle; 12 % loss after 2nd	~93 %	0.4 wt% glucose, 0.075 g catalyst, 90 °C, 16 bar, 4 h, 700 rpm, 35 mL	29

[a]Values close to 100 % represent systems subject to mass-transport limitations; [b]Not reported.

The superior D-sorbitol selectivity of larger Pt nanoparticles was independent of conversion (**Figure S9**) in contrast to smaller particles wherein selectivity decreased with conversion, suggesting that selective sites within the latter may be lost through reaction-induced restructuring or self-poisoning by reactively-formed adsorbates.

An understanding of the competing pathways leading to D-sorbitol or D-fructose production requires consideration of the factors affecting the conformation of the D-glucose substrate. D-glucose exists in water as a 2:1 ratio of the β-or α-anomer, with only about 0.0026 mol% present as the aldose or ketose open chain forms.[49] D-sorbitol is only produced from the aldose form, attained via proton transfer to the ether-O of the glucopyranose ring and subsequent C(1)-O(5) bond scission (generally considered to be the rate-limiting step in forming the open chain aldose conformation shown in **Scheme 1a**). While the precise mechanism remains under debate, DFT calculations suggest this conformational change initiates in water via deprotonation of the anomeric hydroxyl group, followed by proton transfer to the ring ether-oxygen atom.[50,51] The aldehyde function of the aldose conformer may adsorb on metal surfaces via either the oxygen lone pair η^1_O or carbonyl $\eta^2_{C=O}$ configurations. The latter configuration is favored for allylic aldehydes such as cinnamaldehyde or crotonaldehyde over (111) facets of large Pt particles, promoting C=O bond activation and hydrogenation,[52-55] whereas low coordination (100) and (110) sites prevalent on particles <2 nm promote decarbonylation and concomitant CO self-poisoning.[53] The observed selectivity dependence for D-glucose hydrogenation to D-sorbitol is consistent with these principles, with larger Pt nanoparticles possessing a higher density of (111) facets and hence hydrogenation of the C=O group within the aldose conformer. The higher D-fructose selectivity of smaller Pt nanoparticles may result from preferential coordination of the more weakly bound η^1_O configuration to electron deficient Lewis acid sites (known to catalyze D-glucose isomerization[56]) present over small Pt nanoparticles, which XPS shows possess a higher surface density of $Pt^{\delta+}$ species. DFT calculations also suggest isomerization may be promoted via hydrogen bonding to surface hydroxyls[57] present at the Pt-silica interface. Models of glucose interacting with single Pt atoms on single walled carbon nanotubes show the sugar coordinates via the O atom of the $–C(6)H_2OH$ through charge transfer from glucose→Pt[58] (**Scheme 1b)**.

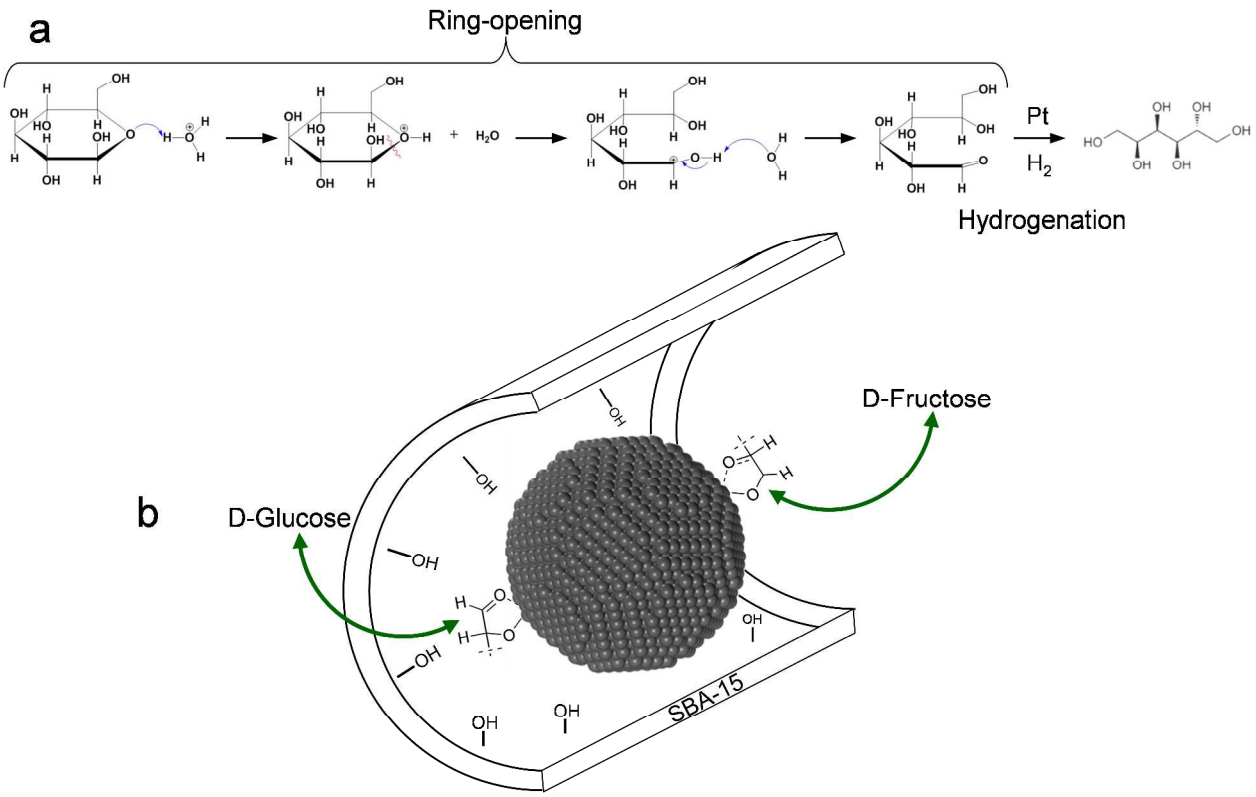

Scheme 1: a) Ring opening and hydrogenation of D-glucose, b) proposed isomerization of D-glucose to D-fructose over low coordination sites of Pt nanoparticles.

In light of the inverse correlation between D-fructose and D-sorbitol production during glucose conversion, the question arises as to whether the latter is formed by the direct hydrogenation of (the aldose conformer of) glucose or an isomerized D-fructose intermediate. Hence, the reactivity of the most selective 1.5 wt% Pt/SBA-15 catalyst towards D-fructose hydrogenation, and the hydro-isomerization of mannitol and sorbitol at 140 °C and 40 bar H_2 was therefore explored subsequently. Whereas D-glucose proceeds almost exclusively to D-sorbitol and D-fructose with 69 % and 30 % selectivity respectively (**Figure S10a**), D-mannitol was the major product of D-fructose hydrogenation (**Figure S10b**), with only 24 % selectivity to D-sorbitol. D-fructose isomerization to D-glucose, and dehydration to 5-HMF were also observed. The overall reaction network for D-glucose hydrogenation, and of the key products/reactive intermediates, is summarized in **Scheme 2**, with the associated rates representing the first intrinsic kinetic parameters for Pt catalyzed glucose hydrogenation, free from mass transport limitations. Negligible hydro-isomerization of D-sorbitol and D-mannitol occurred over our Pt catalysts, with only 6 % and 3% converted respectively after 4 h reaction; hence neither would be anticipated to

undergo interconversion if formed during D-glucose hydrogenation. The superior rate (and selectivity) for D-sorbitol formation from D-glucose in comparison to that for D-mannitol formation from D-fructose, may reflect more sterically-demanding surface constraints associated with the hydrogenation of the latter ketose (versus aldose) conformer. DFT calculations suggest that aldehyde (propanal) hydrogenation should be favored relative to ketone (acetone) hydrogenation over Pt(111) due to the latter adopting the weaker η^1_O adsorption configuration.[59] Consistent with this hypothesis, Heinen et al proposed that the furanose form of fructose binds more weakly than the aldose form of D-glucose,[32] in accordance with our observations for their different rates of hydrogenation.

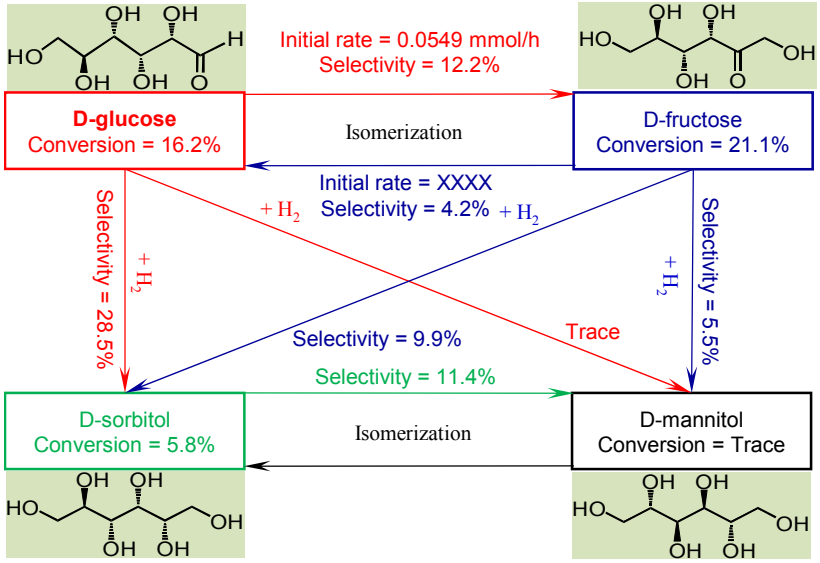

Scheme 2: Reaction network for D-glucose and D-fructose hydrogenation over 1.5 wt% Pt/SBA-15 at 140 °C and 40 bar H_2.

ii) Influence of reaction conditions

Reaction conditions were varied with a view to shedding more insight into the reaction pathways and optimizing D-sorbitol production over the most selective 1.5 wt% Pt/SBA-15 catalyst. **Figure 4** shows the impact of reaction temperature on the rate of glucose conversion and product selectivity. Higher temperatures exponentially increased activity, but favored D-fructose over D-sorbitol, with selectivity to the latter desired product falling from 100 % at 80 °C to a plateau of ~55 % >140 °C (**Figure S11a**), a similar temperature dependent decrease to that observed over Pt/C.[31] The emergence of trace D-mannitol at the highest temperatures is

consistent with a high activation barrier to D-fructose hydrogenation. It is important to note that the overall carbon mass balance decreases significantly at high temperatures (**Figure S11b**), indicating the occurrence of side reactions such as retro-aldols to form dihydroxyacetone, glycol aldehyde and formaldehyde, D-glucose dimerization,[60] and polymerization to solid organic residues (humins).[61,43] Such mass balances and by-product formation are rarely reported or quantified accurately in the literature. Low reaction temperatures therefore favor the selective hydrogenation of D-glucose over Pt, with high temperatures promoting undesirable D-glucose isomerization to fructose and concomitant polymerization and degradation pathways. The apparent activation energy for D-glucose hydrogenation of 47 kJ.mol^{-1} (**Figure S12**) is in good agreement with that of 55 kJ.mol^{-1} for Ru/C,[62] 44 kJ.mol^{-1} for Raney Ni,[9] 67 kJ.mol^{-1} for supported Ni,[12] and 33 kJ.mol^{-1} over Ru/H-Y[14] catalysts.

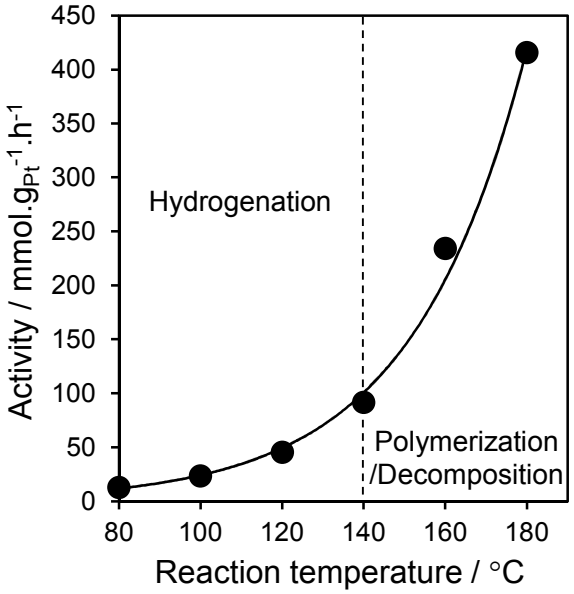

Figure 4. Influence of reaction temperature on the aqueous phase hydrogenation of D-glucose over 1.5 wt% Pt/SBA-15 under 40 bar H_2.

The rate of D-glucose conversion was first order with respect to its concentration for dilute mixtures <10 wt%, deviating only slightly from linearity at higher concentration (**Figure S13a**).[46] Although the selectivity to principal D-sorbitol and D-fructose products was essentially independent of [D-glucose], mass balance fell steeply with increasing substrate concentration (**Figures S13b-c**) in line with reports by Guo et al,[22] likely associated with enhanced solution

phase processes in competition with heterogeneous catalysis. Our observations are in good agreement with previous studies that suggest D-glucose hydrogenation follows Langmuir-Hinshelwood kinetics with first-order behavior for concentrations < 25 wt%,[24,62] with hydrogen dissociation uninhibited by a high D-glucose surface coverage. The pressure dependence of D-glucose conversion was also explored for H_2 pressures spanning 5-60 bar (**Figures 5** and **S14**): activity increased more than ten-fold as the pressure was initially increased from 5 to 10 bar, exhibiting a slower dependence on pressure between 10-40 bar H_2. The reaction order in pH_2 of 0.66 was in reasonable agreement with that expected for a Langmuir-Hinshelwood mechanism requiring dissociative H_2 chemisorption (**Figure S14b**).[63] Similar pressure dependences are reported >10 bar H_2 for D-glucose conversion over Raney Ni[64] and Ru[62, 22] catalysts, although in these instances first order kinetics were claimed, possibly indicative of reactor operation in a diffusion-limited regime.[62] Increasing the hydrogen pressure from 5 to 20 bar induced a switchover in selectivity from predominantly D-fructose to D-sorbitol, suggesting that the D-glucose isomerization pathway is inhibited over H_2 saturated surfaces, which conversely (and unsurprisingly) favor the competing hydrogenation pathway. Carbon mass balances were independent of hydrogen pressure (**Figure S14c**), which we infer therefore exerted minimal influence on side reactions. Qualitatively similar behavior was observed for the lowest loading 0.04 wt% Pt/SBA-15 catalyst (comprising 3.8 nm particles), for which the order with respect to pH_2 was 0.9, and an increase in hydrogen pressure from 40→60 bar enhanced sorbitol selectivity from 12→15 % (i.e. a similar factor to that observed in **Figure 5**).

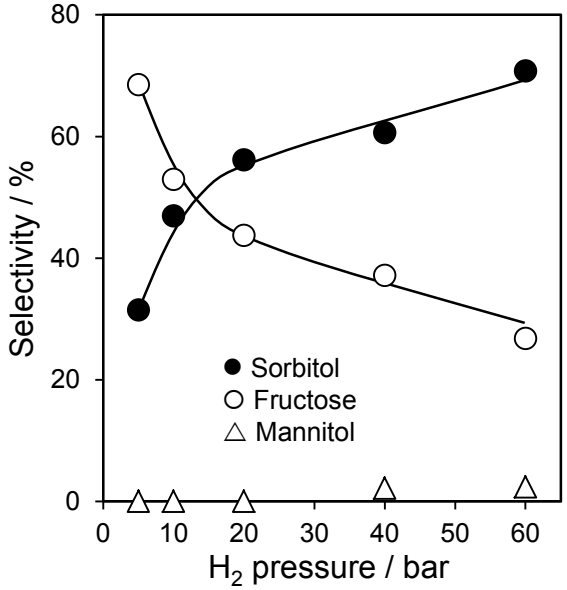

Figure 5: Influence of H_2 pressure on relative product selectivity during the aqueous phase hydrogenation of D-glucose over 1.5 wt% Pt-SBA-15 catalyst at 140 °C. Selectivities calculated at 5 % glucose conversion.

In summary electronically-polarized Pt surfaces/interfaces favor the adsorption and activation of D-glucose molecules via C=O of the aldose form, leading to the formation of an active and selective precursor to D-sorbitol.[11 22] The selectivity to D-sorbitol strongly depends upon the reaction temperature, which could also lead to the isomerization of D-glucose to D-fructose, which can subsequently lead to an increase in the selectivity/yield of D-mannitol. Therefore, on the basis of the above-mentioned results, it should be sensible to conclude that shorter reaction time, lower D-glucose concentration, lower reaction temperature, higher H_2 pressure, and catalyst mass offers the best selectivity to D-sorbitol and a higher mass balance.[17]

4. CONCLUSIONS

Structure-activity relations in the aqueous phase hydrogenation of D-glucose to D-sorbitol were systematically investigated for Pt nanoparticles supported over either low area fumed silica or high area mesoporous SBA-15 supports. D-sorbitol productivity via hydrogenation of the ring-opened aldose form of D-glucose was structure insensitive for Pt particles between 3-17 nm diameter, whereas competing D-glucose isomerization to D-fructose was favored by small, electron deficient Pt particles; both reaction pathways proceeded independently of the choice of silica support. Moderate reaction temperatures <140 °C and high hydrogen pressures suppress D-glucose isomerization to D-fructose (and its subsequent polymerization), maximizing D-sorbitol productivity. D-mannitol does not epimerize to D-sorbitol under our reaction conditions. Our observation that large Pt nanoparticles and high p_{H2} favor selective C=O hydrogenation to the corresponding alcohols is in accordance with related studies on allylic and benzylic aldehydes,[55] implying that particle size effects in Pt catalyzed selective C=O hydrogenations are a generic phenomenon.

ASSOCIATED CONTENT

Supporting Information. Catalyst synthesis procedure and characterization data, along with full details of catalytic reaction data is supplied as Supporting Information. This material is available free of charge via the Internet at http://pubs.acs.org."

AUTHOR INFORMATION

Corresponding Authors

E-mail: a.f.lee@aston.ac.uk; k.wilson@aston.ac.uk.

Author Contributions

The manuscript was written through contributions of all authors. All authors have given approval to the final version of the manuscript.

Funding Sources

This research was supported by the EPSRC and UK Catalysis Hub under grants EP/K014749/1 and EP/K014706/1, and the British Council through the Global Innovation Initiative under the GB3-Net project.

REFERENCES

(1) Lee, A. F.; Bennett, J. A.; Manayil, J. C.; Wilson, K. *Chem. Soc. Rev.* **2014**, *43*, 7887.
(2) Wilson, K.; Lee, A. F. In *Advances in Biorefineries*; Waldron, K., Ed.; Woodhead Publishing: 2014, p 624.
(3) van Putten, R.-J.; van der Waal, J. C.; de Jong, E.; Rasrendra, C. B.; Heeres, H. J.; de Vries, J. G. *Chem. Rev.* **2013**, *113*, 1499.
(4) Climent, M. J.; Corma, A.; Iborra, S. *Green Chem.* **2011**, *13*, 520.
(5) Tai, Z.; Lee, A. F.; Wilson, K. In *Reaction Pathways and Mechanisms in Thermocatalytic Biomass Conversion I: Cellulose Structure, Depolymerization and Conversion by Heterogeneous Catalysts*; Schlaf, M., Zhang, C. Z., Eds.; Springer Singapore: Singapore, 2016, p 123.
(6) Zhang, J.; Li, J.-b.; Wu, S.-B.; Liu, Y. *Ind. Eng. Chem. Res.* **2013**, *52*, 11799.
(7) Vilcocq, L.; Cabiac, A.; Especel, C.; Guillon, E.; Duprez, D. *Oil Gas Sci. Technol.* **2013**, *68*, 841.
(8) Wang, Y.; De, S.; Yan, N. *Chem. Commun.* **2016**, *52*, 6210.
(9) Brahme, P. H.; Doraiswamy, L. K. *Ind. Eng. Chem. Process Des. Dev.* **1976**, *15*, 130.
(10) Wisnlak, J.; Simon, R. *Ind. Eng. Chem. Prod. RD* **1979**, *18*, 50.
(11) Gallezot, P.; Cerino, P. J.; Blanc, B.; Flèche, G.; Fuertes, P. *J. Catal.* **1994**, *146*, 93.
(12) Kusserow, B.; Schimpf, S.; Claus, P. *Adv. Synth. Catal.* **2003**, *345*, 289.
(13) Liu, J.; Bai, P.; Zhao, X. S. *PCCP* **2011**, *13*, 3758.
(14) Mishra, D. K.; Dabbawala, A. A.; Park, J. J.; Jhung, S. H.; Hwang, J.-S. *Catal. Today* **2014**, *232*, 99.
(15) Zhang, J.; Lin, L.; Zhang, J.; Shi, J. *Carbohydr. Res.* **2011**, *346*, 1327.
(16) Sapunov, V. N.; Grigoryev, M. Y.; Sulman, E. M.; Konyaeva, M. B.; Matveeva, V. G. *J. Phys. Chem. A* **2013**, *117*, 4073.
(17) Gallezot, P.; Nicolaus, N.; Flèche, G.; Fuertes, P.; Perrard, A. *J. Catal.* **1998**, *180*, 51.
(18) Perrard, A.; Gallezot, P.; Joly, J.-P.; Durand, R.; Baljou, C.; Coq, B.; Trens, P. *Appl. Catal. A* **2007**, *331*, 100.
(19) Déchamp, N.; Gamez, A.; Perrard, A.; Gallezot, P. *Catal. Today* **1995**, *24*, 29.

(20) Weiss, J. *T. Faraday Soc.* **1941**, *37*, 782.
(21) Arena, B. J. *Appl. Catal. A* **1992**, *87*, 219.
(22) Guo, H.; Li, H.; Zhu, J.; Ye, W.; Qiao, M.; Dai, W. *J. Molec. Catal. A* **2003**, *200*, 213.
(23) Li, H.; Wang, W.; Fa Deng, J. *J. Catal.* **2000**, *191*, 257.
(24) Li, H.; Deng, J.-F. *J. Chem. Tech. Biotech.* **2001**, *76*, 985.
(25) Bratlie, K. M.; Lee, H.; Komvopoulos, K.; Yang, P.; Somorjai, G. A. *Nano Lett.* **2007**, *7*, 3097.
(26) Lordi, V.; Yao, N.; Wei, J. *Chem. Mater.* **2001**, *13*, 733.
(27) Zhang, X.; Liu, P.; Wu, Y.; Yao, Y.; Wang, J. *Catal Lett* **2010**, *137*, 210.
(28) Giang, C.; Osatiashtiani, A.; dos Santos, V.; Lee, A.; Wilson, D.; Waldron, K.; Wilson, K. *Catalysts* **2014**, *4*, 414.
(29) Tathod, A.; Kane, T.; Sanil, E. S.; Dhepe, P. L. *J. Molec. Catal. A* **2014**, *388–389*, 90.
(30) Lazaridis, P. A.; Karakoulia, S.; Delimitis, A.; Coman, S. M.; Parvulescu, V. I.; Triantafyllidis, K. S. *Catal. Today* **2015**, *257, Part 2*, 281.
(31) Liu, C. W.; Zhang, C. H.; Liu, K. K.; Wang, Y.; Fan, G. X.; Sun, S. K.; Xu, J.; Zhu, Y. L.; Li, Y. W. *Biomass Bioenerg.* **2015**, *72*, 189.
(32) Heinen, A. W.; Peters, J. A.; van Bekkum, H. *Carbohydr. Res.* **2000**, *328*, 449.
(33) West, R. M.; Tucker, M. H.; Braden, D. J.; Dumesic, J. A. *Catal. Commun.* **2009**, *10*, 1743.
(34) Kon, K.; Onodera, W.; Shimizu, K. *Catal. Sci. Technol.* **2014**, *4*, 3227.
(35) Cai, H. L.; Li, C. Z.; Wang, A. Q.; Zhang, T. *Catal. Today* **2014**, *234*, 59.
(36) Fukuoka, A.; Dhepe, P. L. *Angew. Chem. Int.-Ed.* **2006**, *45*, 5161.
(37) Kobayashi, H.; Ito, Y.; Komanoya, T.; Hosaka, Y.; Dhepe, P. L.; Kasai, K.; Hara, K.; Fukuoka, A. *Green Chem.* **2011**, *13*, 326.
(38) Wilson, K.; Lee, A. F. *Philos. Trans. A Math. Phys. Eng.* **2016**, *374*.
(39) Durndell, L. J.; Parlett, C. M. A.; Hondow, N. S.; Wilson, K.; Lee, A. F. *Nanoscale* **2013**, *5*, 5412.
(40) Chen, R.; Chen, Z.; Ma, B.; Hao, X.; Kapur, N.; Hyun, J.; Cho, K.; Shan, B. *Comp. Theor. Chem.* **2012**, *987*, 77.
(41) Longwitz, S. R.; Schnadt, J.; Vestergaard, E. K.; Vang, R. T.; Stensgaard, I.; Brune, H.; Besenbacher, F. *J. Phys. Chem. B* **2004**, *108*, 14497.
(42) Maris, E. P.; Ketchie, W. C.; Oleshko, V.; Davis, R. J. *J. Phys. Chem. B* **2006**, *110*, 7869.
(43) De Bruijn, J. M.; Kieboom, A. P. G.; Bekkiun, H. V. *J. Carbohydr. Chem.* **1986**, *5*, 561.
(44) Patil, S. K. R.; Lund, C. R. F. *Energy Fuels* **2011**, *25*, 4745.
(45) Guo, X.; Wang, X.; Guan, J.; Chen, X.; Qin, Z.; Mu, X.; Xian, M. *Chinese J. Catal.* **2014**, *35*, 733.
(46) Mishra, D. K.; Lee, J.-M.; Chang, J.-S.; Hwang, J.-S. *Catal. Today* **2012**, *185*, 104.
(47) Ahmed, M. J. *Heat Mass Transf.* **2012**, *48*, 343.
(48) Kanie, Y.; Akiyama, K.; Iwamoto, M. *Catal. Today* **2011**, *178*, 58.
(49) Qian, X. *J. Phys. Chem. B* **2013**, *117*, 11460.
(50) Plazinski, W.; Plazinska, A.; Drach, M. *PCCP* **2015**, *17*, 21622.
(51) Trinh, Q. T.; Chethana, B. K.; Mushrif, S. H. *J. Phys. Chem. C* **2015**, *119*, 17137.
(52) Zhao, H.; Kim, J.; Koel, B. E. *Surf. Sci.* **2003**, *538*, 147.
(53) Grass, M. E.; Rioux, R. M.; Somorjai, G. A. *Catal Lett* **2009**, *128*, 1.
(54) Prashar, A. K.; Mayadevi, S.; Nandini Devi, R. *Catal. Commun.* **2012**, *28*, 42.
(55) Durndell, L. J.; Parlett, C. M. A.; Hondow, N. S.; Isaacs, M. A.; Wilson, K.; Lee, A. F. *Sci. Rep.* **2015**, *5*.

(56) Chatterjee, C.; Pong, F.; Sen, A. *Green Chem.* **2015**, *17*, 40.
(57) Yang, G.; Pidko, E. A.; Hensen, E. J. M. *ChemSusChem* **2013**, *6*, 1688.
(58) Ganji, M. D.; Emami Skardi, F. S. *FULLER NANOTUB CAR N* **2015**, *23*, 273.
(59) Alcalá, R.; Greeley, J.; Mavrikakis, M.; Dumesic, J. A. *J. Chem. Phys.* **2002**, *116*, 8973.
(60) Schimpf, S.; Louis, C.; Claus, P. *Appl. Catal. A* **2007**, *318*, 45.
(61) Delidovich, I.; Palkovits, R. *Catal. Sci. Technol.* **2014**, *4*, 4322.
(62) Crezee, E.; Hoffer, B. W.; Berger, R. J.; Makkee, M.; Kapteijn, F.; Moulijn, J. A. *Appl. Catal. A* **2003**, *251*, 1.
(63) Olivas, A.; Jerdev, D. I.; Koel, B. E. *J. Catal.* **2004**, *222*, 285.
(64) Hoffer, B. W.; Crezee, E.; Mooijman, P. R. M.; van Langeveld, A. D.; Kapteijn, F.; Moulijn, J. A. *Catal. Today* **2003**, *79–80*, 35.

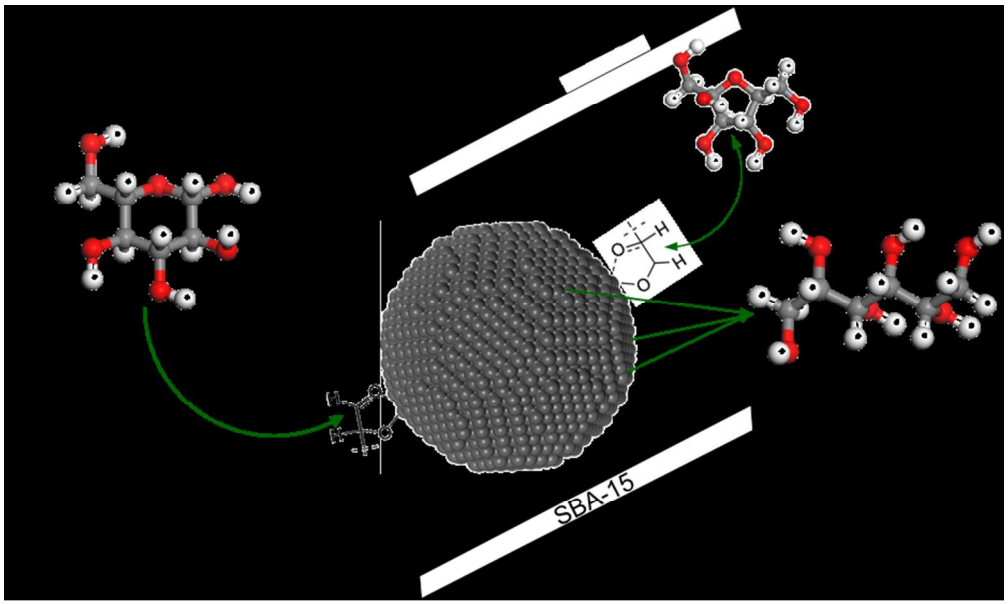

Platinum catalyzed glucose hydrogenation to sorbitol is structure insensitive and competes with structure-sensitive isomerization to fructose.

157x93mm (150 x 150 DPI)